
Neural Architecture Generator Optimization

Binxin Ru

Machine Learning Research Group
University of Oxford, UK
robin@robots.ox.ac.uk

Pedro M. Esperança

Huawei Noah's Ark Lab
London, UK
pedro.esperanca@huawei.com

Fabio M. Carlucci

Huawei Noah's Ark Lab
London, UK
fabio.maria.carlucci@huawei.com

Abstract

Neural Architecture Search (NAS) was first proposed to achieve state-of-the-art performance through the discovery of new architecture patterns, without human intervention. An over-reliance on expert knowledge in the search space design has however led to increased performance (local optima) without significant architectural breakthroughs, thus preventing truly novel solutions from being reached. In this work we propose 1) to cast NAS as a problem of finding the optimal network generator and 2) a new, hierarchical and graph-based search space capable of representing an extremely large variety of network types, yet only requiring few continuous hyper-parameters. This greatly reduces the dimensionality of the problem, enabling the effective use of Bayesian Optimisation as a search strategy. At the same time, we expand the range of valid architectures, motivating a multi-objective learning approach. We demonstrate the effectiveness of our strategy on six benchmark datasets and show that our search space generates extremely lightweight yet highly competitive models illustrating the benefits of a NAS approach that optimises over network generator selection. The code is available at https://github.com/rubinxin/vega_NAGO.

1 Introduction

Neural Architecture Search (NAS) has the potential to discover paradigm-changing architectures with state-of-the-art performance, and at the same time removes the need for a human expert in the network design process. While significant improvements have been recently achieved [1, 2, 3, 4, 5, 6], this has taught us little about *why* a specific architecture is more suited for a given dataset. Similarly, no conceptually new architecture structure has emerged from NAS works. We attribute this to two main issues: (i) reliance on over-engineered search spaces and (ii) the inherent difficulty in analyzing complex architectures.

The first point is investigated in [7]. In order to reduce search time, current NAS methods often restrict the macro-structure and search only the micro-structure at the cell level, focusing on which operations to choose but fixing the global wiring pattern [1, 8, 9, 10]. This leads to high accuracy but restricts the search to local minima: indeed deep learning success stories, such as ResNet [11], DenseNet [12] and Inception [13] all rely on specific global wiring rather than specific operations.

The second issue appears hard to solve, as analyzing the structure of complex networks is itself a demanding task for which few tools are available. We suggest that by moving the focus towards *network generators* we can obtain a much more informative solution, as the whole network can

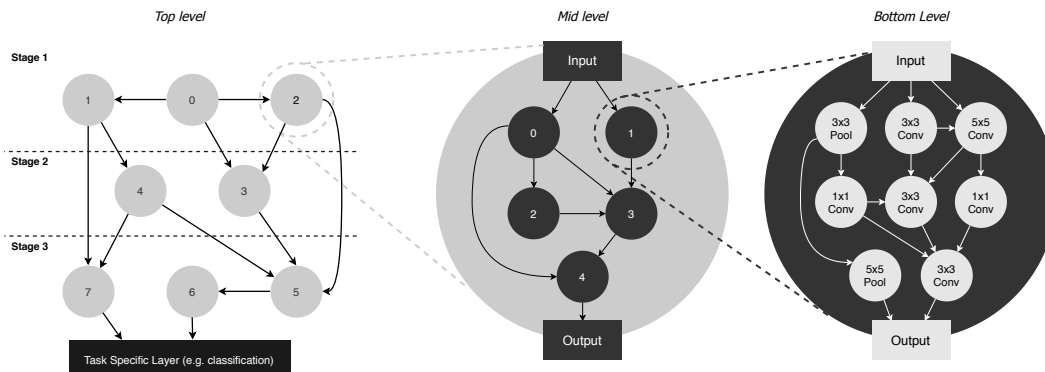


Figure 1: Architecture sampled from HNAG, given hyperparameters Θ . Each node, both in the top-level and mid-level graphs, is an independently sampled graph. Finally, at the bottom level each node corresponds to an independently sampled atomic operation. Note how features at the top level can flow between different stages (e.g. from node 1 and 4 to 7), which is beneficial for certain tasks.

then be represented by a small set of parameters. This idea, first introduced by [14], offers many advantages for NAS: the smaller number of parameters is easier to optimize and easier to interpret when compared to the popular categorical, high-dimensional search spaces. Furthermore it allows the algorithm to focus on macro differences (e.g. global connectivity) rather than the micro differences arising from minor variations with little impact on the final accuracy.

To summarize, our main contributions are as follows.

- 1) A **Network Architecture Generator Optimization framework** (NAGO), which redirects the focus of NAS from optimizing a single architecture to optimizing an architecture generator. To the best of our knowledge, we are the first to investigate this direction and we demonstrate the usefulness of this by using Bayesian Optimization (BO) in both multi-fidelity and multi-objective settings.
- 2) A new **hierarchical, graph-based search space**, together with a stochastic network generator which can output an extremely wide range of previously unseen networks in terms of wiring complexity, memory usage and training time.
- 3) **Extensive empirical evaluation** showing that NAGO achieves state-of-the-art NAS results on a variety of vision tasks, and finds lightweight yet competitive architectures.

2 Neural Architecture Generator

Previous research has shown that small perturbations in the network’s structure do not significantly change its performance, i.e. the specific connection between any single pair of nodes is less important than the overall connectivity [14, 7]. As such, we hypothesize, and experimentally confirm in Section 4.1, that architectures sampled from the same generative distribution perform similarly. This assumption allows us to greatly simplify the search and explore more configurations in the search space by only evaluating those sampled from different generator hyperparameters. Therefore, instead of optimizing a specific architecture, we focus on finding the optimal hyperparameters for a stochastic network generator [14].

2.1 Hierarchical Graph-based Search Space (HNAG)

Our network search space is modelled as a hierarchical graph with three levels (Figure 1). At the top-level, we have a graph of cells. Each cell is itself represented by a mid-level graph. Similarly, each node in a cell is a graph of basic operations (conv 3×3 , conv 5×5 , etc.). This results in 3 sets of graph hyperparameters: θ_{top} , θ_{mid} , θ_{bottom} , each of which independently defines the graph generation model in each level. Following [14] we use the Watts-Strogatz (WS) model as the random graph generator for the top and bottom levels, with hyperparameters $\theta_{top} = [N_t, K_t, P_t]$ and $\theta_{bottom} = [N_b, K_b, P_b]$; and use the Erdős-Rényi (ER) graph generator for the middle level, with hyperparameters $\theta_{mid} = [N_m, P_m]$ to allow for the single-node case¹. This gives us the flexibility to reduce our search space to two levels (when the mid-layer becomes single node) and represent a

¹The WS model cannot generate a single-node graph but the ER model can.

DARTS-like architecture. Indeed HNAG is designed to be able to emulate existing search spaces while also exploring potentially better/broader ones.

By varying the graph generator hyperparameters and thus the connectivity properties at each level, we can produce a extremely diverse range of architectures (see end of this section). For instance, if the top-level graph has 20 nodes arranged in a feed-forward configuration and the mid-level graph has a single node, then we obtain networks similar to those sampled from the DARTS search space [1]. While if we fix the top-level graph to 3 nodes, the middle level to 1 and the bottom-level graph to 32, we can reproduce the search space from [14].

Stages. CNNs are traditionally divided into stages, each having a different image resolution and number of channels [15, 1, 14]. In previous works, both the length of each stage and the number of channels were fixed. Our search space is the first that permits the learning of the optimal channel ratio as well as the channel multiplier for each stage. To do so, we define two hyperparameter vectors: stage ratio θ_S and channel ratio θ_C . θ_S is normalized and represents the relative length of each stage. For example, if there are 20 nodes at the top level and $\theta_S = [0.2, 0.2, 0.6]$ then the three stages will have 4, 4 and 12 nodes, respectively. θ_C controls the number of channels in each stage; e.g. if it is set to $[4, 1, 4]$ than stages 1 and 3 hold the same number of channels while stage 2 only holds one fourth of that. The absolute number of channels depends on the overall desired number of parameters while θ_C only controls the relative ratio.

Merging options and Operations. When multiple edges enter the same node, they are merged. Firstly, all activations are downscaled via pooling to match the resolution of the smallest tensor. Note we only tried pooling for our work but strided convolution is an alternative option to achieve the same effect. Likewise, we use 1×1 convolutions to ensure that all inputs share the same number of channels. Then, independently for each node, we sample, according to the probability weights θ_M , one merging strategy from: weighted sum, attention weighted sum, concatenation. Each atomic operation is sampled from a categorical distribution parameterized with θ_{op} , which can be task specific.

Therefore, our search space is fully specified by the hyperparameters $\Theta = [\theta_{top}, \theta_{mid}, \theta_{bottom}, \theta_S, \theta_C, \theta_M, \theta_{op}]$. The top-level enables a mixture of short- and long-range connections among features of different stages (resolutions/channels). The mid-level regulates the search complexity of the bottom-level graph by connecting features computed locally (within each mid-level node).² This serves a function similar to the use of cells in other NAS method but relaxes the requirement of equal cells. Our hierarchical search expresses a wide variety of networks (see Section 4.1). The total number of networks in our search space is larger than 4.58×10^{56} . For reference, in the DARTS search space that number is $8^{14} \approx 4.40 \times 10^{12}$ (details in Appendix A).

2.2 BO-based Search Strategy

Our proposed hierarchical graph-based search space allows us to represent a wide variety of neural architectures with a small number of continuous hyperparameters, making NAS amenable to a wide range of powerful BO methods such as multi-fidelity and multi-objective BO. The general algorithm for applying BO to our search space is presented in Appendix B.

Multi-fidelity BO (BOHB). We use the multi-fidelity BOHB approach [16], which uses partial evaluations with smaller-than-full budget in order to exclude bad configurations early in the search process, thus saving resources to evaluate more promising configurations and speeding up optimisation. Given the same time constraint, BOHB evaluates many more configurations than conventional BO which evaluates all configurations with full budget.

Multi-objective BO (MOBO). We use MOBO to optimize for multiple objectives which are conflicting in nature. For example, we may want to find architectures which give high accuracy but require low memory. Given the competing nature of the multiple objectives, we adapt a state-of-the-art MOBO method to learn the Pareto front [17]³. The method constructs multiple acquisition functions, one for each objective function, and then recommends the next query point by sampling the point with

²For example, a 32-nodes graph has 496 possible connections. If we divide this into 4 subgraphs of 8 nodes, that number is $118 = 28 \times 4$ (within subgraphs) + 6 (between subgraphs).

³Note modifying BOHB to also accommodate the multi-objective setting is an interesting future direction. One potential way is to do so by selecting the Pareto set points at each budget to be evaluated for longer epochs during Successive Halving.

the highest uncertainty on the Pareto front of all the acquisition functions. We modify the approach in the following two aspects for our application:

1) *Heteroscedastic surrogate model.* We use a stochastic gradient Hamiltonian Monte Carlo (SGHMC) BNN [18] as the surrogate, which does a more Bayesian treatment of the weights and thus gives better-calibrated uncertainty estimates than other alternatives in prior BO-NAS works [19, 20, 21]. SGHMC BNN in [18] assumes homoscedastic aleatoric noise with zero mean and constant variance w_n^2 . By sampling the network weights w_f and the noise parameter w_n from their posterior $w^i \sim p(w|D)$ where $w = [w_f, w_n]$ and D is the surrogate training data, the predictive posterior mean $\mu(f|\Theta, D)$ and variance $\sigma^2(f|\Theta, D)$ are approximated as:

$$\mu(f|\Theta, D) = \frac{1}{N} \sum_{i=1}^N \hat{f}(\Theta; w_f^i), \quad \sigma^2(f|\Theta, D) = \frac{1}{N} \sum_{i=1}^N \hat{f}(\Theta; w_f^i)^2 - \mu(f|D)^2 + w_n^2 \quad (1)$$

However, our optimization problem has heteroscedastic aleatoric noise: the variance in the network performance, in terms of test accuracy or other objectives, changes with the generator hyperparameters (Figure 2). Therefore, we propose to append a second output to the surrogate network and model the noise variance as a deterministic function of the inputs, $w_n^2(\Theta)$. Our heteroscedastic BNN has the same predictive posterior mean as Equation (2.2) but a slightly different predictive posterior variance: $\sigma^2(f|\Theta, D) = \frac{1}{N} \sum_{i=1}^N \left(\hat{f}(\Theta; w_f^i)^2 + (w_n^i(\Theta))^2 \right) - \mu(f|\Theta, D)^2$. Our resultant surrogate network comprises 3 fully-connected layers, each with 10 neurons, and two outputs. The hyperparameter details for our BNN surrogate is described in Appendix C.

We verify the modelling performance of our heteroscedastic surrogate network by comparing it to its homoscedastic counterpart. We randomly sample 150 points from BOHB query data for each of the five image datasets and randomly split them into a train-test ratio of 1:2. The median results on negative log likelihood (NLL) and root mean square error (RMSE) over 10 random splits are shown in Table 1. The heteroscedastic model not only improves over the homoscedastic model on RMSE, which depends on the predictive posterior mean only, but more importantly, shows much lower NLL, which depends on both the predictive posterior mean and variance. This shows that the heteroscedastic surrogate can model the variance of the objective function better, which is important for the BO exploration.

2) *Parallel evaluations per BO iteration.* The original multi-objective BO algorithm is sequential (i.e. recommends one new configuration per iteration). We modify the method to a batch algorithm which recommends multiple new configurations per iteration and enjoys faster convergence in terms of BO iterations [22, 23]. This allows the use of parallel computation to evaluate batches of configurations simultaneously. We collect the batch by applying the local penalisation on the uncertainty metric of the original multi-objective BO [23]. See Appendix D for details.

Table 1: Regression performance of heteroscedastic (Het) and homoscedastic (Hom) BNN surrogates, trained on 50 generator samples and tested on 100 samples, in terms of negative log-likelihood (NLL) and root mean square error (RMSE)

	NLL		RMSE	
	Hom	Het	Hom	Het
CIFAR10	5.92	3.43	0.02	0.01
CIFAR100	7.15	0.89	0.02	0.02
SPORT8	23.8	19.0	0.15	0.14
MIT67	7.23	-0.92	0.12	0.11
FLOWERS102	15.6	7.49	0.19	0.18

3 Related Work

Neural Architecture Search (NAS). NAS aims to automate the design of deep neural networks and was initially formulated as a search problem over the possible operations (e.g. convolutions and pooling filters) in a graph. Several approaches have been proposed that outperform human-designed networks in vision tasks: reinforcement learning [24, 3], evolution [25], gradient descent [1, 8] and multi-agent learning [4]. To achieve a computationally feasible solution, these works rely on a manually-designed, cell-based search space where the macro-structure of the network (the global *wiring*) is fixed and only the micro-structure (the *operations*) is searched. Some recent works also start to look into the search space design [26, 27] but study very different perspectives from our work.

Network Wiring. Recent works have explored the importance of the wiring of a neural network. [28] use a gradient-based approach to search the network wiring via learnable weights, and [29]

search for the wirings among channels instead of layers; both modify existing network architectures instead of discovering new ones. In contrast, [14] build networks from random graph models.

The concept of stochastic network generator was introduced by [14] who show that networks based on simple random graph models (RNAG) are competitive with human and algorithm designed architectures on the ImageNet benchmark. In contrast with our work, they do not offer a strategy to optimize their generators. The second main difference with their work lies in our search space (HNAG). While RNAG is *flat* with 3 sequentially connected graphs, HNAG is *hierarchical* with each node in the higher level corresponding to a graph in the level below, leading to a variable number of nested graphs. Our 3-level hierarchical structure is not only a generalization which enables the creation of more complex architectures, but it also allows the creation of local clusters of operation units, which result in more memory efficient models (Fig.3) or architectures with fewer nodes (Sec.4.3). Moreover, the HNAG top level provides diverse connections across different stages, leading to more flexible information flow than RNAG. Finally, nodes in RNAG only process features of fixed channel size and resolution within a stage while those in HNAG receive features with different channel sizes and resolution. To summarize, our work distinguishes itself by proposing a significantly different search space *and* a BO based framework to optimize it, empirically evaluating it on 6 datasets and further investigating the multi-objective setting [6, 30].

BO for NAS. BO has been widely used for optimizing the hyperparameters of machine learning algorithms [31, 32, 33, 34, 35, 16, 36] and more recently it has found applications in NAS [37, 38, 19, 20, 21]. However, current NAS search spaces—even cell-based ones—are noncontinuous and relatively high dimensional [39], thus unfavourable to conventional BO algorithms that focus on low-dimensional continuous problems [40, 41]. Our proposed HNAG which addresses the above issues can make NAS amenable to BO methods.

Hierarchical Search Space. [42] proposes to search for the outer network-level structure in addition to the commonly searched cell-level structure; [43] proposes a factorised hierarchical search space which permits different operations and connections in different cells; [44] introduce a hierarchical construction of networks with higher-level motifs being formed by using lower-level motifs. However, none of these prior works propose to optimise architecture generators instead of single architectures, which is the main contribution of our search space; Such generator-based search space formulation leads to advantages like high expressiveness, representational compactness and stochasticity.

4 Experiments

We experiment with the following two network generators.

1) Hierarchical Neural Architecture Generator (**HNAG**): our proposed 3-level, hierarchical generator. Due to resource constraint, we limit our search space to the 8 *random graph generator hyperparameters* $[\theta_{top}, \theta_{mid}, \theta_{bottom}]^4$. The search ranges of these hyperparameters are in Appendix E. Following [14] we fix $\theta_S = [0.33, 0.33, 0.33]$ and $\theta_C = [1 : 2 : 4]$. Experiments on expanded search spaces are shown in Appendix H. The absolute number of channels for each stage is computed by multiplying the channel ratio with a constant which is calculated based on our parameter limit.

2) Randomly Wired Neural Architecture Generator (**RNAG**): the flat network generator in [14] which connects three WS graphs in sequence to form an architecture. We optimize the three WS hyperparameters (N, K, P) for each stage, leading to 9 hyperparameters in total.

For both HNAG and RNAG, we apply multi-fidelity and multi-objective BO to optimize their hyperparameters, leading to 4 methods for comparison: HNAG-BOHB, HNAG-MOBO, RNAG-BOHB, RNAG-MOBO. To verify the effectiveness of our search strategy as well as expressiveness, we also evaluate the performance of random samples drawn from HNAG (HNAG-RS) and use it as another baseline. For all generator-based methods, we use summation to merge the inputs and only use 3×3 convolution as the operation choice, unless otherwise stated.

Datasets. We perform experiments on a variety of image datasets: CIFAR10, CIFAR100 [45], IMAGENET [46] for object recognition; SPORT8 for action recognition [47]; MIT67 for scene

⁴Namely the 3 WS graph hyperparameters at top and bottom levels, $\theta_{top} \in \mathbb{R}^3$, $\theta_{bottom} \in \mathbb{R}^3$; and the 2 ER graph hyperparameters at mid level, $\theta_{mid} \in \mathbb{R}^2$.

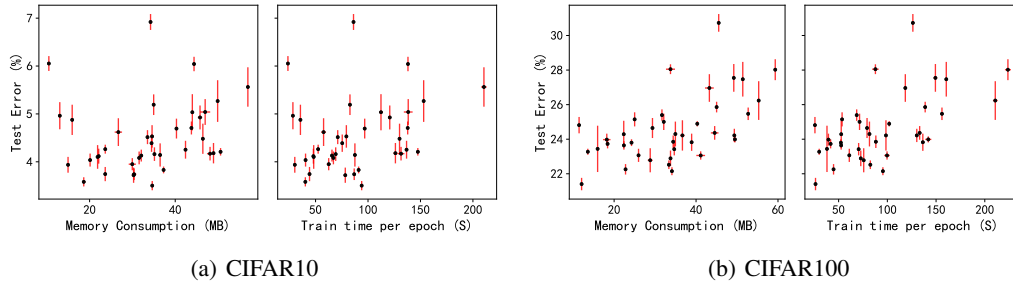


Figure 2: Expressiveness of our HNAG search space. The above plots shows the mean and standard deviation of test error vs. memory consumption and training time per epoch achieved by 40 random generator hyperparameters for CIFAR10 and CIFAR100. The mean and standard deviation of results over the 8 sampled architectures for each generator hyperparameter are presented.

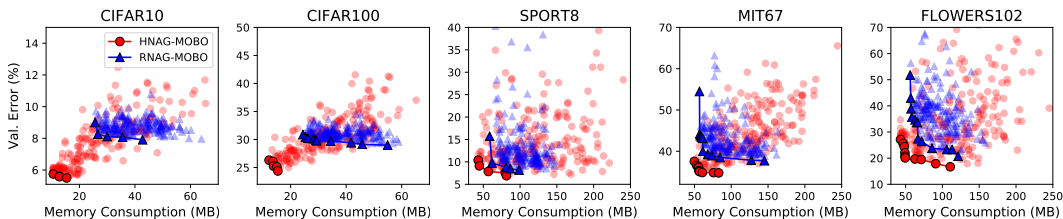


Figure 3: Query data by MOBO for HNAG (red) and RNAG (blue). The Pareto optimal configurations are highlighted in solid lines and filled markers. Each BO evaluation uses 200 training epochs for SPORT8 and 60 training epochs for the other datasets.

recognition [48]; FLOWERS102 for fine-grained object recognition [49]. We limit the number of network parameters to 4.0M for small-image tasks and 6.0M for large-image tasks.

Complete training protocol. For all datasets except IMAGENET, we evaluate the performance of the (Pareto) optimal generators recommended by BO by sampling 8 networks from the generator and training them to completion (600 epochs) with initial learning rate 0.025 and batch size 96. For IMAGENET, we follow the complete training protocol of small model regime in [14], which trains the networks for 250 epochs with an initial learning rate of 0.1 and a batch size of 256. We use dropout with length 16 for small-image tasks and size 112 for large-image tasks. Note that we do not use DropPath or other advanced training augmentations. All experiments use NVIDIA Tesla V100 GPUs.

4.1 Expressiveness of the search space

We evaluate the performance of 40 randomly sampled network generator hyperparameters for CIFAR10 and CIFAR100 (Figure 2). The performance of each hyperparameter set is evaluated by training 8 neural network architectures generated by following the complete training protocol (described above) and evaluating on the test datasets. Similar plots following the training protocol in the BO search phase are presented in Appendix G. There are three observations we highlight.

Firstly, the accuracy (test error) and efficiency (memory consumption⁵ or training time) achieved by different generator hyperparameters are spread over a considerable range. This shows that our search space can express a variety of generators whose networks have different characteristics, thus optimization is meaningful. Secondly, the networks produced by good generator hyperparameters mostly have small variation in their accuracy and memory, which justifies our proposal to focus on the generator instead of the network. It also supports our approach to assess the performance of a specific generator configuration with only one architecture sample in our BO phase. Third, there exist Pareto optimal generator hyperparameters in our search space as some of them result in architectures which are both efficient and accurate. This justifies our motivation for performing MOBO.

⁵See Appendix F for a comparison with DARTS search space.

Table 2: Validation accuracy (%) and search cost (GPU days) for BOHB results. The accuracy reported is obtained in the BOHB search setting which uses large batch sizes based on GPU machine memory and trains the network sample for 400 epochs for SPORT8 and 120 epochs for the other datasets.

	RNAG-BOHB		HNAG-BOHB	
	Accuracy	Cost	Accuracy	Cost
CIFAR10	93.5	14.0	95.6	12.8
CIFAR100	72.2	11.8	77.2	10.4
SPORT8	94.7	23.4	95.3	17.6
MIT67	67.7	22.6	71.8	20.0
FLOWERS102	91.4	11.2	93.3	10.6

Table 3: The optimal values found for the 8 generator hyperparameters for single-objective BOHB (top block) and MOBO (bottom block) experiments. ‘‘MPS’’ is Memory Per Sample.

	Top			Mid		Bottom			MPS (MB)
	N	K	P	N	P	N	K	P	
CIFAR10	8	5	0.6	1	0.7	5	4	0.2	17
CIFAR100	8	5	0.4	1	0.7	4	2	0.4	14
SPORT8	7	2	0.9	5	0.8	6	3	0.6	121
MIT67	9	4	0.6	1	0.2	3	2	0.5	54
FLOWERS102	6	4	0.4	1	0.4	6	5	0.9	62
IMAGENET	4	2	0.5	5	0.6	6	4	0.4	136
CIFAR10	6	4	0.8	1	0.1	3	2	0.5	13
CIFAR100	6	4	0.3	1	0.7	3	2	0.5	13
SPORT8	3	2	0.3	1	0.2	3	2	0.8	43
MIT67	3	2	0.6	1	0.8	4	2	0.6	48
FLOWERS102	6	5	0.2	1	0.8	3	2	0.5	48

Table 4: Test accuracy (%) and memory consumption (MB) for variants of HNAG and RNAG after completing training. ‘‘BOHB’’ and ‘‘MOBO’’ indicates BO was used to optimise generator hyperparameters. ‘‘RNAG-D’’ is the best generator in [14] and ‘‘HNAG-RS’’ is the generator with hyperparameters randomly sampled from HNAG. Each table entry shows ‘‘mean (stdev)’’ of test accuracy (top row) and memory (bottom row) over 8 random samples. The best performance, separately for test accuracy and memory consumption, is highlighted in bold. Number of model parameters is limited to 4M for CIFAR10 and CIFAR100 and 6M for the other datasets.

	RNAG-BOHB	HNAG-BOHB	RNAG-MOBO	HNAG-MOBO	RNAG-D	HNAG-RS
CIFAR10	94.3(0.13) 57.9(0.52)	96.6(0.15) 17.0(1.76)	94.0(0.26) 25.9(0.91)	96.6(0.07) 12.8(0.00)	94.1(0.16) 44.2(1.29)	95.7(0.68) 53.9(40.6)
CIFAR100	73.0(0.50) 56.5(0.90)	79.3(0.31) 14.0(1.07)	71.8(0.50) 27.0(0.91)	77.6(0.45) 12.8(0.00)	71.7(0.36) 43.5(1.23)	77.1(1.34) 72.6(40.2)
SPORT8	93.6(0.76) 101.9(1.18)	94.9(0.52) 121.9(13.1)	93.1(0.73) 57.8(1.07)	95.2(0.40) 43.1(0.00)	93.6(0.99) 112.1(3.45)	93.2(1.55) 375.7(277)
MIT67	68.3(0.78) 156.1(6.40)	74.2(0.67) 54.1(2.50)	66.9(1.46) 56.7(0.59)	73.5(0.56) 48.1(0.00)	66.7(0.54) 111.7(3.58)	72.5(1.38) 324.8(140)
FLOWERS102	95.7(0.38) 143.5(2.27)	97.9(0.18) 61.7(0.00)	94.9(0.53) 63.0(1.63)	98.1(0.19) 48.4(0.00)	94.7(0.46) 111.6(3.35)	95.3(1.29) 211.2(140)

4.2 BO Experiments

BOHB is used to find the optimal network generator hyperparameters in terms of the validation accuracy. We perform BOHB for 60 iterations. We use training budgets of 100, 200, 400 epochs to evaluate architectures on SPORT8 and 30, 60, 120 epochs on the other datasets. MOBO returns the Pareto front of generator hyperparameters for two objectives: validation accuracy and sample memory. For parallel MOBO, we start with 50 BOHB evaluation data and search for 30 iterations with a BO batch size of 8; at each BO iteration, the algorithm recommends 8 new points to be evaluated and updates the surrogate model with these new evaluations. We use a fixed training budget of 200 epochs to evaluate architectures suggested for SPORT8 and 60 epochs for the other datasets. For experiments with both BO methods, we only sample 1 architecture to evaluate the performance of a specific generator. We scale the batch size up to a maximum of 512 to fully utilise the GPU memory and adjust the initial learning rate via linear extrapolation from 0.025 for a batch size of 96 to 0.1 for a batch size of 512. The other network training set-up follows the complete training protocol.

The validation accuracy of the best generator configuration recommended by BOHB as well as the computation costs to complete the BOHB search for both our proposed hierarchical network generator (HNAG) and the Randomly Wired Networks Generator (RNAG) are shown in Table 2. HNAG improves over RNAG in terms of both accuracy and cost. The high rank correlation between architecture accuracies at subsequent budgets (see Fig. 5b in Appendix I) indicates that a good generator configuration remains good even when a new architecture is re-sampled and re-evaluated at a higher budget; this reconfirms the validity of our practice to assess the generator configuration performance with only one architecture sample during the BO search phase.

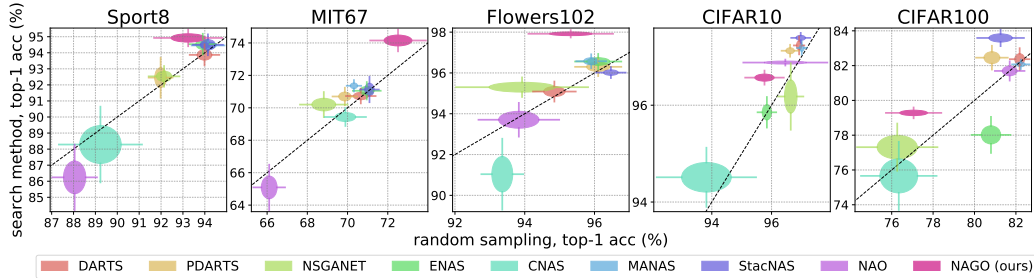


Figure 4: Comparison of various NAS methods (performance on y-axis) and random sampling (performance on x-axis) from their respective search spaces. Ellipse centres, ellipse edges and whisker ends represent the $\mu \pm \{0, \sigma/2, \sigma\}$, respectively (mean μ , standard deviation σ). Methods above the diagonal line outperform the average architecture, and vice-versa. Note NAGO clearly achieves the largest improvement over naive random sampling than all other methods on all tasks. Results for all methods except ours (NAGO: HNAG-BOHB) were taken from public resources provided by [7]. While all high-performing competing methods use Cutout, DropPath and Auxiliary Towers, our method only uses Cutout. The other methods are: DARTS [1], PDARTS [2], NSGANET [50], ENAS [3], CNAS [51], MANAS [4], StacNAS [5], NAO [52].

The query data by MOBO over the two objectives, validation error and sample memory consumption are presented in Figure 3. Clearly, the Pareto front of HNAG dominates that of RNAG, showing that our proposed search space not only performs better but is also more memory efficient.

4.3 Analysis of the Optimal Hyperparameters

In Table 3, most optimal generators have much fewer nodes (≤ 40 nodes) than the graph-based generator in [14] (96 nodes) while still achieve better performance (Section 4.4). This shows that our hierarchical search space helps reduce the complexity/size of the architectures found. Interestingly, most datasets have the optimal solution with a single-node mid-level graph. We hypothesize this to be due to the low parameter count we enforced, which encourages the search to be conservative with the total number of nodes. Moreover, we see similar configurations appear to be optimal for different datasets, showing the promise of using transfer-learning to speed up the search in our future work.

4.4 Complete Training Results

We train (i) the best network generator hyperparameters of both HNAG and RNAG found by BO; (ii) the default optimal RNAG setting (RNAG-D) recommended in [14]; and (iii) randomly sampled hyperparameters values for our HNAG (HNAG-RS) following the complete training protocol. HNAG clearly outperforms RNAG (Table 4). Moreover, in the multi-objective case, HNAG-MOBO is able to find models which are not only competitive in test accuracy but also very lightweight (i.e., consuming only 1/3 of the memory when compared to RNAG-D).

Table 5: Test accuracy (%) of small networks ($\sim 6M$ parameters) on IMAGENET. We train our HNAG-BOHB for 250 epochs similar to RandomWire-WS [14].

Network	Top-1 acc.	Top-5 acc.	Params(M)
ShuffleNetV2 [53]	74.9	92.2	7.4
NASNet [54]	74.0	91.6	5.3
Amoeba [55]	75.7	92.4	6.4
PNAS [56]	74.2	91.9	5.1
DARTS [1]	73.1	91.0	4.9
XNAS [8]	76.0	—	5.2
RandWire-WS	74.7	92.2	5.6
HNAG-BOHB	76.8	93.4	5.7

An interesting analysis is presented in Figure 4. This plot shows the relationship between randomly-sampled and method-provided architectures, and is thus able to separate the contribution of the search space from that of the search algorithm. Notably, not only does NAGO provide high accuracy, but also has the best relative improvements of all methods. It must be noted that while these methods train their networks using Cutout [57], DropPath [58] and Auxiliary Towers [13], *we only used Cutout*. DropPath and Auxiliary Towers could conceivably be used with our search space ⁶, although an effective and efficient implementation is non-trivial. Furthermore, the competitive performance of

⁶We naively apply DropPath and Auxiliary Towers, following set-ups in [1], to re-train architectures from our hierarchical search space. These techniques lead to 0.54% increase in the average test accuracy 25 over 8 architecture samples on CIFAR10, leading to results competitive with the state-of-the-art.

one-shot NAS methods is largely due to the above-mentioned training techniques and their well-designed narrow search space [7]. Finally, while the number of parameters in other methods can vary quite a lot (the number of channels is fixed, regardless of the specific solution), NAGO dynamically computes the appropriate number of channels to preserve the given parameter count.

We also perform the search on IMAGENET. Due to resource constraints, we only run 10 iterations of BOHB with search budgets of 15, 30, 60 epochs and train 2 sample networks from the best generator hyperparameters recommended by BOHB, following the complete training protocol in [14]. Although this is likely a sub-optimal configuration, it serves to validate our approach on large datasets such as IMAGENET. The mean network performance achieved by HNAG-BOHB approach outperforms [14] and other benchmarks (Table 5). Note that XNAS uses DropPath, Auxiliary Towers and AutoAugment [59] to boost performance.

5 Discussion and conclusion

We presented NAGO, a novel solution to the NAS problem. Due to its highly-expressive hierarchical, graph-based search space, together with its focus on optimizing a generator instead of a specific network, it significantly simplifies the search space and enables the use of more powerful global optimisation strategies. NAGO, as other sample-based NAS methods, requires more computation (< 20 GPU-days) than one-shot NAS methods (< 2 GPU-days). The later are geared towards fast solutions, but rely heavily on weight-sharing (with associated drawbacks [60]) and a less expressive search space with fixed macro-structure to achieve this speed-up, and tend to overfit to specific datasets (CIFAR), while under-performing on others (Figure 4). Additionally, while the architectures found by NAGO are already extremely competitive, the training protocol is not fully optimised: NAGO does not use DropPath or Auxiliary Towers—which have been used to significantly boost performance of one-shot NAS [7]—so additional accuracy gains are available, and we aim to transfer these protocols to our HNAG backbone. For future direction it would be interesting to consider a lifelong NAS setting or transfer learning, in which each new task can build on previous experience so that we can quickly get good results on large datasets, such as ImageNet. This can be more easily achieved with our novel search space HNAG as it allows us to deploy the existing transfer-learning BO works directly. In addition, the network generator hyperparameters define the global properties of the resultant architectures—network connectivity and operation types—and from these we can derive a high level understanding of the properties that make up a good architecture for a given task.

6 Broader Impact

As highlighted in [7], NAS literature has focused for a long time on achieving higher accuracies, no matter the source of improvement. This has led to the widespread use of narrowly engineered search spaces, in which all considered architectures share the same human defined macro-structure. While this does lead to higher accuracies, it prevents those methods from ever finding truly novel architecture. This is detrimental both for the community, which has focused many works on marginally improving performance in a shallow pond, but also for the environment [61]. As NAS is undoubtedly computationally intensive, researchers have the moral obligation to make sure these resources are invested in meaningful pursuits: our flexible search space, based on hierarchical graphs, has the potential to find truly novel network paradigms, leading to significant changes in the way we design networks. It is worth mentioning that, as our search space is fundamentally different from previous ones, it is not trivial to use the well-optimised training techniques (e.g. DropPath, Auxiliary Towers, etc.) which are commonly used in the field. While transferring those techniques is viable, we do believe that our new search space will open up the development of novel training techniques.

We do however acknowledge that the computational costs of using our NAS approach are still relatively high - this may not be attractive to the industrial or academic user with limited resources. On the other hand, by converting NAS to a low-dimensional hyperparameter optimisation problem, we have significantly reduced the optimisation difficulty and opened up the chance of applying more optimisation techniques to NAS. Although only demonstrated with BOHB and MOBO in this work, we believe more query-efficient methods, such as BO works based on transfer learning [62, 63, 64, 65, 66, 67] can be deployed directly on our search space to further reduce the computation costs.

References

- [1] H. Liu, K. Simonyan, and Y. Yang, “DARTS: Differentiable architecture search,” in *International Conference on Learning Representations (ICLR)*, 2019.
- [2] X. Chen, L. Xie, J. Wu, and Q. Tian, “Progressive differentiable architecture search,” in *International Conference on Computer Vision (ICCV)*, 2019.
- [3] H. Pham, M. Guan, B. Zoph, Q. Le, and J. Dean, “Efficient neural architecture search via parameter sharing,” in *International Conference on Machine Learning (ICML)*, pp. 4092–4101, 2018.
- [4] F. Carlucci, P. M. Esperança, M. Singh, A. Yang, V. Gabillon, H. Xu, Z. Chen, and J. Wang, “MANAS: Multi-agent neural architecture search,” *arxiv:1909.01051*, 2019.
- [5] G. Li, X. Zhang, Z. Wang, Z. Li, and T. Zhang, “StacNAS: Towards stable and consistent optimization for differentiable neural architecture search,” *arXiv:1909.11926*, 2019.
- [6] H. Cai, L. Zhu, and S. Han, “ProxylessNAS: Direct neural architecture search on target task and hardware,” in *International Conference on Learning Representations (ICLR)*, 2019.
- [7] A. Yang, P. M. Esperança, and F. M. Carlucci, “NAS evaluation is frustratingly hard,” in *International Conference on Learning Representations (ICLR)*, 2020.
- [8] N. Nayman, A. Noy, T. Ridnik, I. Friedman, R. Jin, and L. Zelnik, “XNAS: Neural architecture search with expert advice,” in *Advances in Neural Information Processing Systems (NIPS)*, pp. 1975–1985, 2019.
- [9] J. Fang, Y. Sun, K. Peng, Q. Zhang, Y. Li, W. Liu, and X. Wang, “Fast neural network adaptation via parameter remapping and architecture search,” in *International Conference on Learning Representations (ICLR)*, 2020.
- [10] J. Mei, X. Lian, X. Jin, L. Yang, Y. Li, A. Yuille, and J. Yang, “AtomNAS: Fine-grained end-to-end neural architecture search,” in *International Conference on Learning Representations (ICLR)*, 2020.
- [11] K. He, X. Zhang, S. Ren, and J. Sun, “Deep residual learning for image recognition,” in *Computer Vision and Pattern Recognition (CVPR)*, pp. 770–778, 2016.
- [12] G. Huang, Z. Liu, L. Van Der Maaten, and K. Q. Weinberger, “Densely connected convolutional networks,” in *Computer Vision and Pattern Recognition (CVPR)*, pp. 4700–4708, 2017.
- [13] C. Szegedy, W. Liu, Y. Jia, P. Sermanet, S. Reed, D. Anguelov, D. Erhan, V. Vanhoucke, and A. Rabinovich, “Going deeper with convolutions,” in *Computer Vision and Pattern Recognition (CVPR)*, pp. 1–9, 2015.
- [14] S. Xie, A. Kirillov, R. Girshick, and K. He, “Exploring randomly wired neural networks for image recognition,” *arXiv:1904.01569*, 2019.
- [15] C. Szegedy, S. Ioffe, V. Vanhoucke, and A. A. Alemi, “Inception-v4, Inception-ResNet and the impact of residual connections on learning,” in *Conference on Artificial Intelligence (AAAI)*, 2017.
- [16] S. Falkner, A. Klein, and F. Hutter, “BOHB: Robust and efficient hyperparameter optimization at scale,” in *International Conference on Machine Learning (ICML)*, pp. 1436–1445, 2018.
- [17] S. Belakaria, A. Deshwal, N. K. Jayakodi, and J. R. Doppa, “Uncertainty-aware search framework for multi-objective Bayesian optimization,” in *Conference on Artificial Intelligence (AAAI)*, 2020.
- [18] J. T. Springenberg, A. Klein, S. Falkner, and F. Hutter, “Bayesian optimization with robust Bayesian neural networks,” in *Advances in Neural Information Processing Systems (NIPS)*, pp. 4134–4142, 2016.
- [19] L. Ma, J. Cui, and B. Yang, “Deep neural architecture search with deep graph Bayesian optimization,” in *Web Intelligence (WI)*, pp. 500–507, IEEE/WIC/ACM, 2019.
- [20] H. Shi, R. Pi, H. Xu, Z. Li, J. T. Kwok, and T. Zhang, “Multi-objective neural architecture search via predictive network performance optimization,” 2019.
- [21] C. White, W. Neiswanger, and Y. Savani, “BANANAS: Bayesian optimization with neural architectures for neural architecture search,” *arXiv:1910.11858*, 2019.

- [22] J. González, Z. Dai, P. Hennig, and N. Lawrence, “Batch bayesian optimization via local penalization,” in *Artificial Intelligence and Statistics (AISTATS)*, pp. 648–657, 2016.
- [23] A. S. Alvi, B. Ru, J. Calliess, S. J. Roberts, and M. A. Osborne, “Asynchronous batch Bayesian optimisation with improved local penalisation,” *arXiv:1901.10452*, 2019.
- [24] B. Zoph and Q. Le, “Neural architecture search with reinforcement learning,” in *International Conference on Learning Representations (ICLR)*, 2017.
- [25] E. Real, S. Moore, A. Selle, S. Saxena, Y. L. Suematsu, J. Tan, Q. V. Le, and A. Kurakin, “Large-scale evolution of image classifiers,” in *International Conference on Machine Learning (ICML)*, pp. 2902–2911, 2017.
- [26] G. Bender, H. Liu, B. Chen, G. Chu, S. Cheng, P.-J. Kindermans, and Q. V. Le, “Can weight sharing outperform random architecture search? an investigation with tunas,” in *Proceedings of the IEEE/CVF Conference on Computer Vision and Pattern Recognition*, pp. 14323–14332, 2020.
- [27] I. Radosavovic, R. P. Kosaraju, R. Girshick, K. He, and P. Dollár, “Designing network design spaces,” in *Proceedings of the IEEE/CVF Conference on Computer Vision and Pattern Recognition*, pp. 10428–10436, 2020.
- [28] K. Yuan, Q. Li, Y. Zhou, J. Shao, and J. Yan, “Diving into optimization of topology in neural networks.” OpenReview ID:HyetFnEFDS, 2020.
- [29] M. Wortsman, A. Farhadi, and M. Rastegari, “Discovering neural wirings,” in *Advances in Neural Information Processing Systems (NIPS)*, pp. 2680–2690, 2019.
- [30] T. Elsken, J. H. Metzen, and F. Hutter, “Efficient multi-objective neural architecture search via lamarckian evolution,” in *International Conference on Learning Representations*, 2018.
- [31] J. Snoek, H. Larochelle, and R. P. Adams, “Practical Bayesian optimization of machine learning algorithms,” in *Advances in Neural Information Processing Systems (NIPS)*, pp. 2951–2959, 2012.
- [32] J. S. Bergstra, R. Bardenet, Y. Bengio, and B. Kégl, “Algorithms for hyper-parameter optimization,” in *Advances in Neural Information Processing Systems (NIPS)*, pp. 2546–2554, 2011.
- [33] J. Bergstra, D. Yamins, and D. D. Cox, “Making a science of model search: Hyperparameter optimization in hundreds of dimensions for vision architectures,” in *International Conference on Machine Learning (ICML)*, 2013.
- [34] F. Hutter, H. H. Hoos, and K. Leyton-Brown, “Sequential model-based optimization for general algorithm configuration,” in *Learning and Intelligent Optimization (LION)*, pp. 507–523, 2011.
- [35] A. Klein, S. Falkner, S. Bartels, P. Hennig, and F. Hutter, “Fast Bayesian optimization of machine learning hyperparameters on large datasets,” *arXiv:1605.07079*, 2016.
- [36] Y. Chen, A. Huang, Z. Wang, I. Antonoglou, J. Schrittwieser, D. Silver, and N. de Freitas, “Bayesian optimization in AlphaGo,” *arXiv:1812.06855*, 2018.
- [37] K. Kandasamy, W. Neiswanger, J. Schneider, B. Póczos, and E. P. Xing, “Neural architecture search with Bayesian optimisation and optimal transport,” in *Advances in Neural Information Processing Systems (NIPS)*, pp. 2016–2025, 2018.
- [38] C. Ying, A. Klein, E. Christiansen, E. Real, K. Murphy, and F. Hutter, “NAS-Bench-101: Towards reproducible neural architecture search,” in *International Conference on Machine Learning (ICML)*, pp. 7105–7114, 2019.
- [39] T. Elsken, J. H. Metzen, and F. Hutter, “Neural architecture search: A survey,” *arXiv:1808.05377*, 2018.
- [40] B. Shahriari, K. Swersky, Z. Wang, R. P. Adams, and N. De Freitas, “Taking the human out of the loop: A review of bayesian optimization,” *Proceedings of the IEEE*, vol. 104, no. 1, pp. 148–175, 2015.
- [41] P. Hennig, M. A. Osborne, and M. Girolami, “Probabilistic numerics and uncertainty in computations,” *Proc. R. Soc. A*, vol. 471, no. 2179, p. 20150142, 2015.
- [42] C. Liu, L.-C. Chen, F. Schroff, H. Adam, W. Hua, A. L. Yuille, and F.-F. Li, “Auto-deeplab: Hierarchical neural architecture search for semantic image segmentation,” in *CVPR*, 2019.

- [43] M. Tan, B. Chen, R. Pang, V. Vasudevan, M. Sandler, A. Howard, and Q. Le, “Mnasnet: Platform-aware neural architecture search for mobile,” in *2019 IEEE/CVF Conference on Computer Vision and Pattern Recognition (CVPR)*, pp. 2815–2823, 2019.
- [44] H. Liu, K. Simonyan, O. Vinyals, C. Fernando, and K. Kavukcuoglu, “Hierarchical representations for efficient architecture search,” in *International Conference on Learning Representations*, 2018.
- [45] A. Krizhevsky, “Learning multiple layers of features from tiny images,” tech. rep., University of Toronto, 2009.
- [46] J. Deng, W. Dong, R. Socher, L.-J. Li, K. Li, and L. Fei-Fei, “ImageNet: A large-scale hierarchical image database,” in *Computer Vision and Pattern Recognition (CVPR)*, pp. 248–255, 2009.
- [47] L.-J. Li and L. Fei-Fei, “What, where and who? classifying events by scene and object recognition,” in *International Conference on Computer Vision (ICCV)*, pp. 1–8, 2007.
- [48] A. Quattoni and A. Torralba, “Recognizing indoor scenes,” in *Computer Vision and Pattern Recognition (CVPR)*, pp. 413–420, 2009.
- [49] M.-E. Nilsback and A. Zisserman, “Automated flower classification over a large number of classes,” in *Indian Conference on Computer Vision, Graphics & Image Processing (ICVGIP)*, pp. 722–729, 2008.
- [50] Z. Lu, I. Whalen, V. Boddeti, Y. Dhebar, K. Deb, E. Goodman, and W. Banzhaf, “NSGA-NET: a multi-objective genetic algorithm for neural architecture search,” in *Genetic and Evolutionary Computation Conference (GECCO)*, 2019.
- [51] Y. Weng, T. Zhou, L. Liu, and C. Xia, “Automatic convolutional neural architecture search for image classification under different scenes,” *IEEE Access*, vol. 7, pp. 38495–38506, 2019.
- [52] R. Luo, F. Tian, T. Qin, E. Chen, and T.-Y. Liu, “Neural architecture optimization,” in *Advances in Neural Information Processing Systems (NIPS)*, pp. 7816–7827, 2018.
- [53] N. Ma, X. Zhang, H.-T. Zheng, and J. Sun, “Shufflenet v2: Practical guidelines for efficient cnn architecture design,” in *Proceedings of the European Conference on Computer Vision (ECCV)*, pp. 116–131, 2018.
- [54] B. Zoph, V. Vasudevan, J. Shlens, and Q. V. Le, “Learning transferable architectures for scalable image recognition,” in *Computer Vision and Pattern Recognition (CVPR)*, pp. 8697–8710, 2018.
- [55] E. Real, A. Aggarwal, Y. Huang, and Q. V. Le, “Regularized evolution for image classifier architecture search,” in *Proceedings of the aaai conference on artificial intelligence*, vol. 33, pp. 4780–4789, 2019.
- [56] C. Liu, B. Zoph, M. Neumann, J. Shlens, W. Hua, L.-J. Li, L. Fei-Fei, A. Yuille, J. Huang, and K. Murphy, “Progressive neural architecture search,” in *European Conference on Computer Vision (ECCV)*, pp. 19–34, 2018.
- [57] T. DeVries and G. W. Taylor, “Improved regularization of convolutional neural networks with cutout,” *arXiv:1708.04552*, 2017.
- [58] G. Larsson, M. Maire, and G. Shakhnarovich, “Fractalnet: Ultra-deep neural networks without residuals,” *arXiv:1605.07648*, 2016.
- [59] E. D. Cubuk, B. Zoph, D. Mane, V. Vasudevan, and Q. V. Le, “Autoaugment: Learning augmentation policies from data,” *arXiv:1805.09501*, 2018.
- [60] A. Zela, J. Siems, and F. Hutter, “Nas-bench-1shot1: Benchmarking and dissecting one-shot neural architecture search,” in *International Conference on Learning Representations*, 2020.
- [61] E. Strubell, A. Ganesh, and A. McCallum, “Energy and policy considerations for deep learning in nlp,” *arXiv preprint arXiv:1906.02243*, 2019.
- [62] M. Wistuba, N. Schilling, and L. Schmidt-Thieme, “Two-stage transfer surrogate model for automatic hyperparameter optimization,” in *Joint European conference on machine learning and knowledge discovery in databases*, pp. 199–214, Springer, 2016.
- [63] M. Poloczek, J. Wang, and P. I. Frazier, “Warm starting bayesian optimization,” in *2016 Winter Simulation Conference (WSC)*, pp. 770–781, IEEE, 2016.

- [64] Z. Wang, B. Kim, and L. P. Kaelbling, “Regret bounds for meta bayesian optimization with an unknown gaussian process prior,” in *Advances in Neural Information Processing Systems*, pp. 10477–10488, 2018.
- [65] M. Wistuba, N. Schilling, and L. Schmidt-Thieme, “Scalable gaussian process-based transfer surrogates for hyperparameter optimization,” *Machine Learning*, vol. 107, no. 1, pp. 43–78, 2018.
- [66] M. Feurer, B. Letham, and E. Bakshy, “Scalable meta-learning for bayesian optimization using ranking-weighted gaussian process ensembles,” in *AutoML Workshop at ICML*, 2018.
- [67] V. Perrone, R. Jenatton, M. W. Seeger, and C. Archambeau, “Scalable hyperparameter transfer learning,” in *Advances in Neural Information Processing Systems*, pp. 6845–6855, 2018.
- [68] E. Brochu, V. M. Cora, and N. De Freitas, “A tutorial on bayesian optimization of expensive cost functions, with application to active user modeling and hierarchical reinforcement learning,” *arXiv preprint arXiv:1012.2599*, 2010.
- [69] Z. B. Zabinsky, “Random search algorithms,” *Wiley encyclopedia of operations research and management science*, 2010.

A Comparison of our hierarchical search space (HNAG) with previous ones

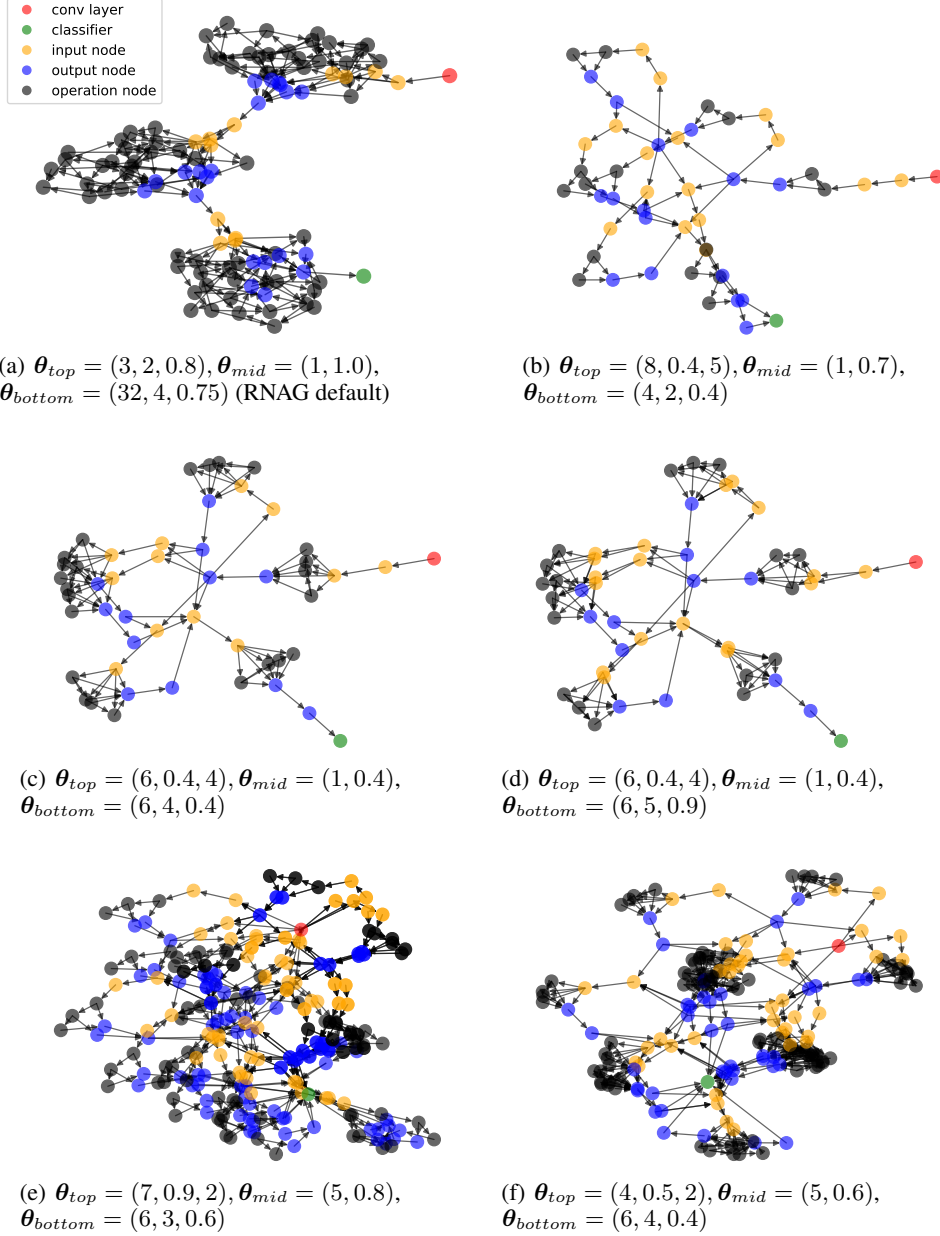


Figure 5: Our proposed HNAG search space contains a large diversity of architectures

A.1 Quantifying the expressiveness of the hierarchical search space (HNAG) against DARTS search space

The total number of possible graphs in our hierarchical search space is larger than

$$T = \underbrace{\left(\sum_{n=3}^{N_O} 2^{\phi(n)} \right)}_{\text{Operation-level}} \cdot \underbrace{\left(\sum_{n=1}^{N_C} 2^{\phi(n)} \right)}_{\text{Cell-level}} \cdot \underbrace{\left(\sum_{n=3}^{N_S} 2^{\phi(n)} \cdot M^n \right)}_{\text{Stage-level}}$$

where $\phi(n) = n(n + 1)/2$ is the number of possible DAGs with n nodes; N_O , N_C , N_S are the maximum numbers of nodes in the operation-, cell- and stage-level graphs, respectively; and M is the number of possible operations in the operation-level graph.

NOTE: This calculation does not include all variations due to the different merging possibilities for each node (addition and concatenation).

Concretely, for the setting implemented ($N_O = N_C = N_S = 10$, $M = 5$) we have $T_{\text{HNAG}} \approx 4.58 \times 10^{56}$. For comparison, the DARTS search space has $T_{\text{DARTS}} = 8^{14} \approx 4.40 \times 10^{12}$.

A.2 Example architectures from HNAG search space

We show six sample architectures drawn from our proposed HNAG search space in Figure 5. It’s evident that our hierarchical graph-based search space can generate a large variety of architectures. Note Figure 5 (a) corresponds to the optimal architecture proposed in [14], which is also contained in our search space.

A.3 Illustrating difference from RNAG [14]

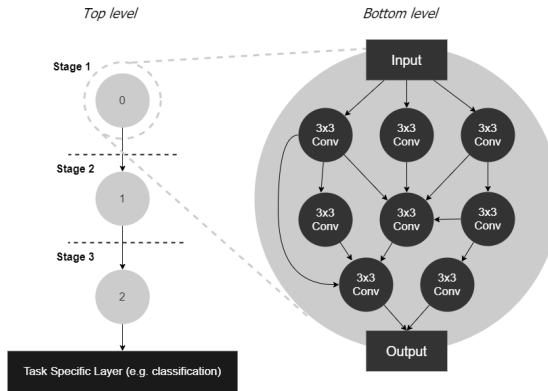


Figure 6: Architecture sampled from RNAG. RNAG is flat but our HNAG is hierarchical.

While RNAG is *flat* with 3 sequentially connected graphs, HNAG is *hierarchical* with 3 levels and each node in the higher level corresponds to a graph in the level below. Thus, the middle graph in RNAG does not correspond to the middle-level graph in HNAG. Our 3-level hierarchical structure is not only a generalisation which enables the creation of more complex architectures, but it also allows the creation of local clusters of operation units, which result in more memory efficient models or architectures with fewer nodes as shown in the main paper and Figure 5. Moreover, the HNAG top level provides diverse connections across different stages, leading to more flexible information flow than RNAG. Finally, nodes in RNAG only process features of fixed channel size and resolution within a stage while those in HNAG receive features with different channel sizes and resolution. To summarize, our proposed search space HNAG is significantly different from RNAG.

B Neural Architecture Generator Optimisation (NAGO) Algorithm

BO is a technique for optimizing a black-box function which is usually noisy and expensive to evaluate. The two key components of BO are: a statistical surrogate model which models the unknown objective; and an acquisition function which is optimized to recommend the next query location [68, 40]. Our NAGO algorithm deploys BO to optimise over the low-dimensional continuous search space of generator hyperparameters. In summary, NAGO trains the surrogate model from query data and uses it to build an acquisition function which trades off exploitation and exploration. At each iteration, NAGO recommends B new generator hyperparameter values by maximizing the acquisition function and updates the surrogate after evaluating these B points. The full algorithm of NAGO is presented in Algorithm 1.

Algorithm 1 Network Architecture Generator Optimization

- 1: **Input:** Network generator G , BO surrogate model $p(f|\Theta, D)$ and acquisition function $\alpha(\Theta|D)$
 - 2: **for** $t = 1$ **to** T **do**
 - 3: Recommend $\{\Theta_t^j\}_{j=1}^B = \arg \max \alpha_{t-1}(\Theta|D)$
 - 4: **for** $j = 1$ **to** B **in parallel do**
 - 5: Sample an architecture from $G(\Theta_t^j)$ and evaluate its validation performance f_t^j
 - 6: **end for**
 - 7: Update D and thus $p(f|\Theta, D)$ with $\{\Theta_t^j, f_t^j\}_{j=1}^B$
 - 8: **end for**
 - 9: Obtain the best performing Θ^* or the Pareto set Θ^*
 - 10: Sample 8 architectures from $G(\Theta^*)$, train them to completion and report their test performance.
-

C Hyperparameters of BO algorithms in NAGO

For experiments with both BO methods, we only sample 1 architecture to evaluate the performance of a specific generator. We scale the batch size up to a maximum of 512 to fully utilise the GPU memory and adjust the initial learning rate via linear extrapolation from 0.025 for a batch size of 96 to 0.1 for a batch size of 512. The other network training set-up follows the complete training protocol described from line 202 to 208 in Section 4.

C.1 BOHB hyperparameters and set-up

We use the released code of BOHB ⁷. We perform BOHB for 60 iterations with its hyperparameter $\eta = 2$. All the other BOHB hyperparameters follow the default setting in [16]. We use training budgets of 100, 200, 400 epochs to evaluate architectures on SPORT8 and 30, 60, 120 epochs on the other datasets.

C.2 Hyperparameters of MOBO and its heteroscedastic Bayesian Neural Network Surrogate

MOBO returns the Pareto front of generator hyperparameters for two objectives: validation accuracy and sample memory. For parallel MOBO, we start with 50 initial data from BOHB queries and search for 30 iterations with a BO batch size of 8; at each BO iteration, the algorithm recommends 8 new points to be evaluated and updates the surrogate model with these new evaluations. We use a fixed training budget of 200 epochs to evaluate architectures suggested for SPORT8 and 60 epochs for the other datasets.

Our Bayesian neural network surrogate is a 3-layer fully connected network with 10 neurons for each layer and two final outputs: predicted validation accuracy and heteroscedastic noise variance. For sampling network weights, we perform $5 \times |D|$ SGHMC steps as burn-in, followed by 10×100 sampling steps (retaining every 10th sample). We use a total of 100 samples of w_f to approximate the integration in Equation (1) in the main paper. All the other hyperparameters of SGHMC follow the default setting in [18]. We implemented this surrogate by modifying the code of [18] ⁸.

D Local Penalisation for Batch Bayesian Optimization

We adopt the hard local penalization method proposed in [23] to collect a batch of new generator configurations which are then evaluated in parallel. The method sequentially selects a batch of B new configurations by repeatedly applying a hard local penalizer function on the selected points (Algorithm 2).

⁷Available at <https://github.com/automl/HpBandSter>

⁸Available at <https://github.com/automl/pybnn>

Algorithm 2 Local Penalisation

- 1: **Input:** BO surrogate model $p(f|\Theta, D)$ and acquisition function $\alpha(\Theta|D)$, BO batch size B , Local penalization function $\phi(\Theta|\Theta^j)$
 - 2: **Output:** The batch of new configurations $\mathcal{B} = \{\Theta^j\}_{j=1}^B$
 - 3: $\Theta^1 = \arg \max \alpha(\Theta|D)$ and $\mathcal{B} = \{\Theta^1\}$
 - 4: **for** $j = 2, \dots, B$ **do**
 - 5: $\Theta^j = \arg \max \left(\alpha(\Theta|D) \prod_{i=1}^{j-1} \phi(\Theta|\Theta^i) \right)$
 - 6: $\mathcal{B} \leftarrow \mathcal{B} \cup \Theta^j$
 - 7: **end for**
-

The hard penalisation function is defined as:

$$\phi(\Theta|\Theta^j) = \min \left\{ \frac{L \|\Theta - \Theta^j\|}{|\mu(f|\Theta, D) - M| + \sigma(f|\Theta, D)}, 1 \right\}$$

where M is the best objective value observed so far, $L = \max_{\Theta} \|\nabla \mu(f|\Theta, D)\|$ is the approximated Lipschitz constant of the objective function, and $\mu(f|\Theta, D)$ and $\sigma(f|\Theta, D)$ are predictive posterior mean and standard deviation of the BO surrogate model.

E Search Range of Generator Hyperparameters

For our Hierarchical Neural Architecture Generator (HNAG), the ranges over which the generator hyperparameters are searched are defined as:

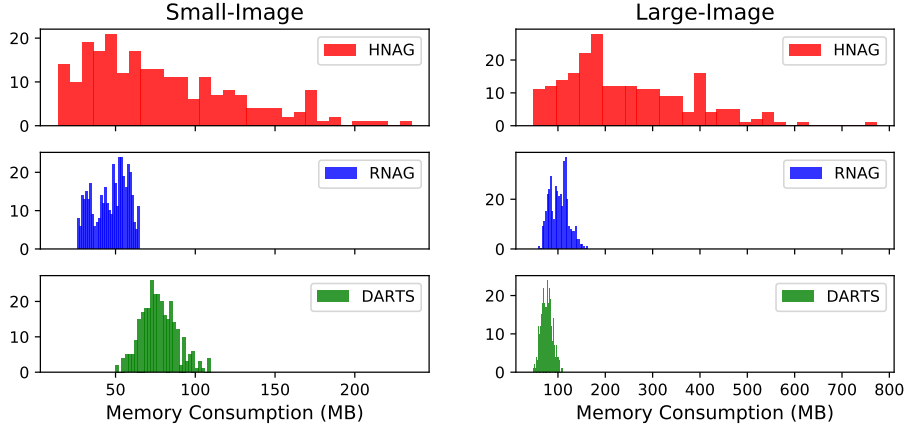


Figure 7: Memory consumption histograms of 300 sample architectures from HNAG, RNAG and DARTS search spaces for small-image $32 \times 32 \times 3$ and large-image $224 \times 224 \times 3$ datasets. Our HNAG search space can generate architectures with a wider range of memory consumption, especially for the large-image data.

Hyperparameters of the top-level and bottom-level Watts–Strogatz graphs

- The number of nodes in the graph $N_t, N_b \in [3, 10]$
- The number of nearest neighbors to which each node is connected in ring topology $K_t, K_b \in [2, 5]$
- the probability of rewiring each edge $P_t, P_b \in [0.1, 0.9]$

Hyperparameters of the Mid-level Erdős–Rényi graph

- The number of nodes in the graph $N_m \in [1, 10]$
- the probability of edge creation $P_m \in [0.1, 0.9]$

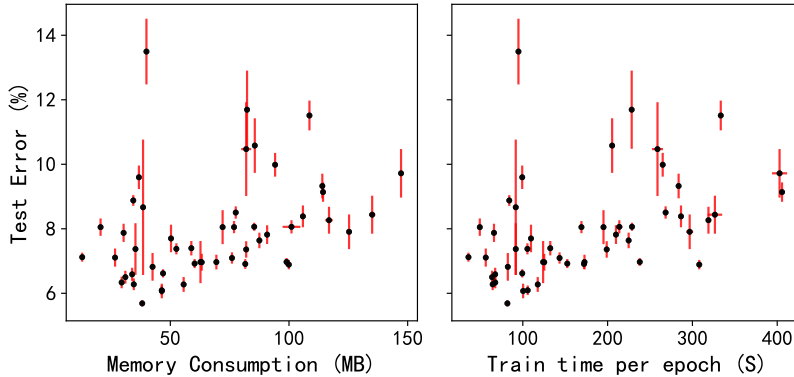


Figure 8: The mean and standard deviation of test error vs. memory consumption and training time per epoch achieved by 50 random generator hyperparameters for CIFAR10 after training for 60 epochs following BO search phase protocol.

For the Randomly Wired Neural Architecture Generator (RNAG), the hyperparameter ranges are:

Hyperparameters of the Watts–Strogatz graphs in 1st, 2nd and 3rd stages

- The number of nodes in the graph $N_1, N_2, N_3 \in [10, 40]$
- The number of nearest neighbors to which each node is connected in ring topology $K_1, K_2, K_3 \in [2, 9]$
- the probability of rewiring each edge $P_1, P_2, P_3 \in [0.1, 0.9]$

Note that although HNAG has a smaller range for the number of nodes in each graph N than RNAG does, it actually can lead to a much larger range of total number of nodes in an architectures ($[9, 1000]$) than that of RNAG ($[30, 120]$).

F Memory Consumption Range of Architectures from Different Search Space

Our hierarchical graph-based search space can generate architectures with a wider range of memory consumption than those of RNAG and DARTS. We draw 300 sample architectures from the search spaces of HNAG, RNAG and DARTS and evaluate their memory consumption per image. The histogram for results on small-image data and large-image data are shown in Figure 7. It is evident that our proposed search space is much wider than both RNAG and DARTS in terms of the memory consumption.

G Performance of randomly sampled network generator hyperparameters during BO search phase

In Figure 8, we evaluate the test performance of 50 randomly sampled network generator hyperparameters for CIFAR10. For each generator hyperparameter value, we sample 8 neural network architectures and train them for 60 epochs following the protocol of the BO search phase: we scale the batch size up to a maximum of 512 to fully utilise the GPU memory and adjust the initial learning rate via linear extrapolation from 0.025 for a batch size of 96 to 0.1 for a batch size of 512. The observations we made on Figure 2 in the main paper also hold for Figure 8.

Table 6: Validation accuracy (%) and search cost (GPU days) for BOHB results. The accuracy reported is obtained in the BOHB search setting which uses large batch sizes based on GPU machine memory and trains the network sample for 400 epochs for SPORT8 and 120 epochs for the other datasets. The search space of HNAG-AugV1 is $\Theta_{augV1} = [\theta_{top}, \theta_{mid}, \theta_{bottom}, \theta_M, \theta_{op}] \in \mathbb{R}^{15}$ while that of HNAG is $\Theta_{origin} = [\theta_{top}, \theta_{mid}, \theta_{bottom}] \in \mathbb{R}^8$.

	HNAG-AugV1		HNAG	
	Accuracy	Cost	Accuracy	Cost
CIFAR10	94.7	19.2	95.6	12.8
CIFAR100	74.5	21.3	77.2	10.4
SPORT8	94.0	26.1	95.3	17.6
MIT67	68.8	33.3	71.8	20.0
FLOWERS102	91.0	14.4	93.3	10.6

H BOHB results on searching more generator hyperparameters

H.1 Include hyperparameters controlling merge options and node operations

We also perform BOHB on an expanded search space Θ_{augV1} which includes not only the original space of the three random graph model hyperparameters $\Theta_{origin} = [\theta_{top}, \theta_{mid}, \theta_{bottom}]$ but also hyperparameters controlling the merge options and node operations θ_M and θ_{op} . Specifically, θ_M defines the probability of choosing weighted sum or concatenation when merging multiple inputs at a node. θ_M defines the probability of choosing a specific operation among (conv1 \times 1, conv3 \times 3, conv5 \times 5, pool3 \times 3 and pool5 \times 5) for each node in the bottom-level graph. The stage ratio and channel ratio are still fixed to $\theta_S = [0.33, 0.33, 0.33]$ and $\theta_C = [1 : 2 : 4]$ following [14]. Therefore, the expanded search space is $\Theta_{augV1} = [\theta_{top}, \theta_{mid}, \theta_{bottom}, \theta_M, \theta_{op}]$.

As seen in Table 6, the best validation accuracies achieved by HNAG-AugV1 are lower than that by HNAG for all the datasets. This result is counter-intuitive as $\Theta_{origin} \subset \Theta_{augV1}$ and thus searching on $\Theta_{expanded}$ should lead to better or at least equal performance as on Θ_{origin} . Yet, this result can be explained by the following two reasons:

- 1) the significant increase in optimisation difficulty. The search dimensionality of Θ_{augV1} is almost twice that of Θ_{origin} , which significantly increases the difficulty of BOHB in finding the global optimum⁹. Thus, given similar search budget, BOHB is more likely to find a hyperparameter near the global optimum or a better local optimum in the space Θ_{origin} than in the expanded space Θ_{augV1} .
- 2) the marginal gain in expanding the search space. [14] empirically demonstrate that the wiring pattern in a architecture plays a much more important role than the operation choices. Our result in Table 6 confirms this observation; namely, after finding the good wiring, changing the operations only lead to small perturbation on the generator performance. Putting this in the context of generator optimisation, it means that the wiring hyperparameters Θ_{origin} determines the region where the global optimum locates and the hyperparameters controlling the operation and merge options only perturb the exact location of the global optimum to a small extent.

Combing the above two factors, we attribute the worse validation performance for HNAG-AugV1V1 to the fact that the increase in optimisation difficulty far outweighs the gain in expanding the search space.

H.2 Include hyperparameters controlling stage ratios and channel ratios

We then perform similar experiments like above but instead optimise the hyperparameters controlling the stage ratios θ_S and channel ratios θ_C while keeping θ_M and θ_{op} fixed. The experimental results are shown in Table 7. While there is a marginal increase in performance, the worst case train time substantially increases due to extreme stage and channel ratios. So, while the number of architectures sampled stays the same, the computational cost increases due to more lengthy training. We had

⁹To optimize a function to within ϵ distance from the global optimum using random search, the expected number of iterations required is $\mathcal{O}(\epsilon^{-d})$ [69]

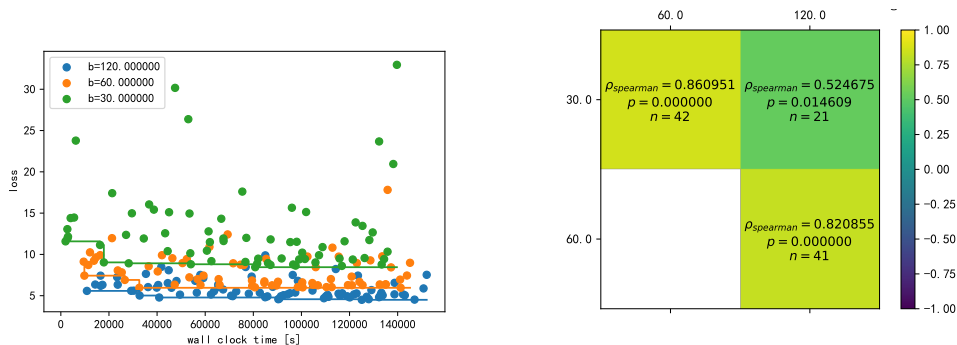
Table 7: Validation accuracy (%) during search and network training time per epoch (seconds). The accuracy reported is obtained in the BOHB search setting which uses large batch sizes based on GPU machine memory and trains the network sample for 400 epochs for SPORT8 and 120 epochs for the other datasets. The search space of HNAG-AugV2 is $\Theta_{augv2} = [\theta_{top}, \theta_{mid}, \theta_{bottom}, \theta_S, \theta_C] \in \mathbb{R}^{14}$ while that of HNAG is $\Theta_{origin} = [\theta_{top}, \theta_{mid}, \theta_{bottom}] \in \mathbb{R}^8$.

	HNAG-AugV2		HNAG	
	Accuracy	Mean(Max) Time	Accuracy	Mean(Max) Time
CIFAR10	95.7	99.3(998)	95.6	54.9(246)
CIFAR100	77.5	82.2(711)	77.2	43.0(216)
SPORT8	95.9	20.6(93.6)	95.3	22.8(37.0)
MIT67	72.0	130(1056)	71.8	85.4(291)
FLOWERS102	93.3	58.4(397)	93.3	45.4(105)

observed this effect during preliminary experiments on CIFAR10 and thus decided to fix θ_S and θ_C to standard values in order to obtain competitive results at a reasonable cost. Nonetheless, even with such constrains on the search space, our HNAG is still much more expressive than most NAS search spaces.

I BOHB samples

Here we show the BOHB query results on the generator hyperparameters for the case of CIFAR10. We use three training budgets in BOHB: 30 (green), 60 (orange) and 120 (blue) epochs. In Figure 9, the top subplot shows the validation error for the three budgets over time. Query data for different budget are mostly well separated. The bottom subplot shows the spearman rank correlation coefficients $\rho_{spearman} \in [-1, 1]$ of the validation errors between different budgets. It’s evident that the $\rho_{spearman}$ between data of 60 epochs and those of 120 epochs are quite high (0.82), indicating that good hyperparameters found in the budget of 60 epochs will remain good when being evaluated with 120 epochs. This motivates our to only a fixed budget of 60 epochs for evaluating all the hyperparameter samples in the multi-objective BO setting.



(a) Validation error for different budgets over time (b) Rank correlation of validation errors across budgets

Figure 9: BOHB query data across different budgets for HNAG on CIFAR10